JOURNAL OF GEOPHYSICAL RESEARCH, VOL. 102, NO. D24, PAGES 29,611–29,624, DECEMBER 26, 1997

Monitoring fire activities in the boreal ecosystem

Zhanqing Li and Josef Cihlar
Canada Centre for Remote Sensing, Ottawa, Ontario, Canada

Louis Moreau and Fengting Huang
Intermap Information Technologies, Ottawa, Ontario, Canada

Bryan Lee
Canadian Forest Service, Edmonton, Alberta, Canada

Abstract. Forest fire is a major disturbance to the boreal ecosystem and may interact with climate change. Unfortunately, we have relatively little knowledge regarding fire activities in the boreal ecosystem. This study investigates the extent and dynamics of the forest fires occurred in and around the Boreal Ecosystem-Atmosphere Study (BOREAS) region during summer 1994, an active fire season on record. The statistics of fire activities were obtained from advanced very high resolution radiometer (AVHRR) (aboard NOAA 11) data employing two satellite-based remote sensing techniques that were designed particularly for monitoring boreal forest fires. Active fires and burned area are estimated using single-day images and 10-day clear composites. Such basic fire attributes as the area and period of burning extracted from the satellite data are compared against the ground reports made by the fire management agencies in Saskatchewan and Manitoba, Canada. Overall, there were 99 fires of a total burning area of approximately 2 million ha found over an area of 800 × 700 km^2 around the BOREAS study region in summer 1994. Agreement in the area of burning is good between the surface observations and satellite-based estimation using single-day images but poor using the composite data that suffer from various uncertainties. The majority (87%) of the ground-reported fires were detected by satellite; the satellite also identified some fires missed by the ground observers. Most fires in 1994 occurred in the transitional forest to the north and northwest of the BOREAS region. Regarding to the monitoring of fire evolution, the daily satellite detection approach can be as effective as or even more effective than ground observations, provided that cloud cover does not occur persistently. The smoke of the fires had an impact on some BOREAS flux measurements.

1. Introduction

A number of recent modeling studies [*Pollard and Thompson*, 1995; *Henderson-Sellers et al.*, 1995] indicate that increasing amounts of greenhouse gases in the atmosphere result in a significant warming and drying of the climate in the boreal forest regions during the summer. These findings coincide with a generally increasing trend of fire activity in boreal forests since the 1950s [*Stocks*, 1991]. For example, five of Canada's most serious fire years in this century occurred after 1980, and the top three years occurred after 1989. Unlike tropical biome burning, which is mostly anthropogenic, a large number of boreal forest fires are naturally induced [*Kasischke et al.*, 1993; *Stocks*, 1991]. Boreal fires are therefore more sensitive to weather and climate than tropical fires. However, fire activities do not show a stable trend on an annual basis because of their highly random nature. Therefore whether the trend of fire activity in the boreal region corroborates the climate change as predicted by models or simply results from natural fluctuation still remains an open question. This issue is further complicated by the fact that damage caused by burning is dictated by fire suppression and other human practices. To unravel the relationship between fire activity and climate change thus entails long-term fire monitoring. Up until now, there have been fewer investigations into fires in the boreal region than in other regions.

Fire is not only affected by weather and climate; it also exerts influence upon the latter by altering solar and terrestrial radiation because of emitted smoke particles and greenhouse gases [*Crutzen et al.*, 1979; *Charlock and Sellers*, 1980; *Kaufman et al.*, 1990a]. In addition to the direct effect of altering the solar radiation budget at the top and bottom of the atmosphere [*Penner et al.*, 1992; *Chylek and Wong*, 1995; *Christopher et al.*, 1996; *Li*, 1997], smoke particles can serve as cloud condensation nuclei, which modify clouds and their radiative properties [*Warner and Twomey*, 1967; *Hobbs and Radke*, 1969; *Hudson et al.*, 1991; *Kaufman and Nakajima*, 1993]. In general, both the direct and indirect effects tend to lower the Earth's surface temperature, as opposed to the warming effect of greenhouse gases released from fires.

Besides, fires release significant amounts of greenhouse gases. A preliminary estimate suggests that the total annual emission due to boreal forest fires amounts to 62.3 Tg of CO_2, 6.3 Tg of CO, 0.7 Tg of CH_4, and other gases [*Stocks*, 1991]. As the goal of the Boreal Ecosystem-Atmosphere Study (BOREAS) is to improve our understanding of the exchange

Published in 1997 by the American Geophysical Union.

Paper number 97JD01106.

of radiation, heat, water, and trace gases between the boreal forest and the lower atmosphere [*Sellers et al.*, 1995], information on fire activity is essential. This is particularly true considering that 1994, the major BOREAS field campaign year, was the third (after 1995 and 1989) most active forest burning year in Canada, with a total area burned of 7.6 million ha; many fires took place near or in the boreal forest region. These fires could significantly affect BOREAS flux measurements. Analysis of these data can thus be facilitated if fire information is available.

Gaining such information by means of space-borne remote sensing is the subject of this study. Ground-based fire observations are employed for validation purpose. The ground data have been extracted from individual wildfire reports prepared by the forest fire management agencies in the provinces of Saskatchewan and Manitoba. Wildfire reports represent the best information available for each individual fire. The quality and accuracy of each report, while variable, are adequate for this study, given the low resolution of the satellite imagery used. Ground data include fire number, location, size, and burning period. The fire location represents the point of ignition for each fire. The total burned area of each fire was estimated primarily from aerial sketch maps which may or may not include unburned islands. Ignition dates are the date of discovery, and while it is quite common for fires to smoulder or "hold over" for one or more days prior to discovery, the fire size at the time of discovery is typically less than 1 ha.

2. Satellite-Based Fire Monitoring Techniques

Remote sensing is an efficient and economical means of monitoring fires over large areas on a routine basis, despite many limitations [*Justice et al.*, 1993]. Satellite observations can provide both the extent of fire scars and the expansion of ongoing fires in time and space [*Robinson*, 1991a]. So far, satellite-based remote sensing of fires has been achieved primarily through the use of passive optical sensors, although microwave measurements by active sensors such as the synthetic aperture radar (SAR) offer certain potential [*Kasischke et al.*, 1994]. The most widely used optical sensor for long-term and large-scale fire monitoring is the advanced very high resolution radiometer (AVHRR) aboard the National Oceanic and Atmospheric Administration's (NOAA) polar orbiting satellites [*Flannigan and Vonder Haar*, 1986; *Kaufman*, 1990a; *Brustet et al.*, 1991a; *Arino and Mellnotte*, 1995], while measurements from many other sensors, such as GOES [*Menzel et al.*, 1991; *Prins and Menzel*, 1994], LANDSAT [*Chuvieco and Congalton*, 1988; *Brustet et al.*, 1991b], and DMSP [*Cahoon et al.*, 1992] have also been employed.

AVHRR has two major advantages for fire monitoring [*Robinson*, 1991b]. First, it provides daily global coverage at a moderate resolution (~1 km), which is critical for operational global monitoring. Second, it has a wide spectral coverage ranging from visible (channel 1, 0.63 μm), near-infrared (channel 2, 0.83 μm), midinfrared (channel 3, 3.4 μm), and thermal wavelengths (channels 4 and 5, 10–12 μm). Each channel pertains to certain attributes of a fire. For example, fire temperature is proportional to thermal radiance in the two infrared channels [*Dozier*, 1981]. The midinfrared channel is more sensitive to the number of fires, as it is saturated even for a very small ignition [*Kaufman et al.*, 1990a; *Robinson*, 1991b]. Smoke is more discernible in the visible channel, and consequently channel 1 measurements may be used to provide information on the loading of smokes [*Kaufman et al.*, 1994]. The extent of total area burned can be assessed, by looking at the difference between the reflectance in the visible and near-infrared channels [*Kasischke et al.*, 1993; *Razafimpanilo et al.*, 1995]. Nevertheless, AVHRR is also subject to numerous shortcomings, notably insufficient diurnal sampling, cloud contamination, and rapid saturation in channel 3 [*Justice et al.*, 1993]. Some of the shortcomings will be overcome by a new generation sensor called the moderate-resolution imaging spectroradiometer (MODIS) on the polar orbiting Earth observation system (Y. J. Kaufman et al., Monitoring global fires from EOS-MODIS, unpublished manuscript, 1997).

This paper deals with the "bulk properties" of the 1994 forest fires, namely, their spatial distribution and temporal evolution, using measurements in AVHRR channels 1, 2, and 3. Following is a brief description of the algorithms used for detecting active fires and burned area from single-day and composite AVHRR data, respectively.

2.1. Algorithm for Detecting Burned Area From 10-day Composite Data

The algorithm is based on the primary observable evidence of the impact of forest fire on remotely sensed signatures. The core information upon which the detection is based is the normalized difference vegetation index (NDVI), defined as the ratio of the difference over the sum of reflectance in AVHRR channels 1 and 2. Following the fire, the NDVI tends to decrease significantly [*Takana et al.*, 1983]. The magnitude of the decrease will depend on the NDVI value before the fire, the fire type (ground or crown), and the degree of burn damage. A decrease in NDVI should thus be observed after a fire, both in individual composites and in the growing season NDVI totals. Ideally, the burn signal should be stronger in the composites obtained shortly after the fire. This is because the difference before and after fire would be most clearly evident in a before-after fire comparison [*Martin and Chuvieco*, 1995]. In practice, however, several significant sources of noise interfere with the signal of burned pixels. These include (1) pervasive smoke during the growing season, especially once fires start and if they are widespread; (2) clouds which obscure pixel information for some composite periods; (3) misregistration of pixels and the tendency of composites to decrease the apparent size of the damaged area (if prepared with the maximum NDVI compositing criterion); (4) variability in the measured NDVI due to inaccuracies in atmospheric and bidirectional reflectance corrections.

Therefore a robust fire detection algorithm must be insensitive to the above sources of noise. An initial algorithm was derived with the use of two parameters quantifying the reduction in NDVI after fire, namely, the magnitude of the NDVI difference before and after fire (FN) and the difference between the area under the NDVI curve during the growing season between the preceding year and the year of interest (FD). The appendix outlines the computation of the two parameters and the procedures of scar detection using these parameters. A distribution showing a pixel-by-pixel plot of FD versus FN for all land pixels is indicative of the degree of burn damage. In particular, heavily burned forest should have large values of FN, especially if the burn took place near the peak green part of the growing season, and large FD. In Figure 1 one can see an example of this skewed distribution for some burns in 1994. Use of the two parameters (FN and FD) helps

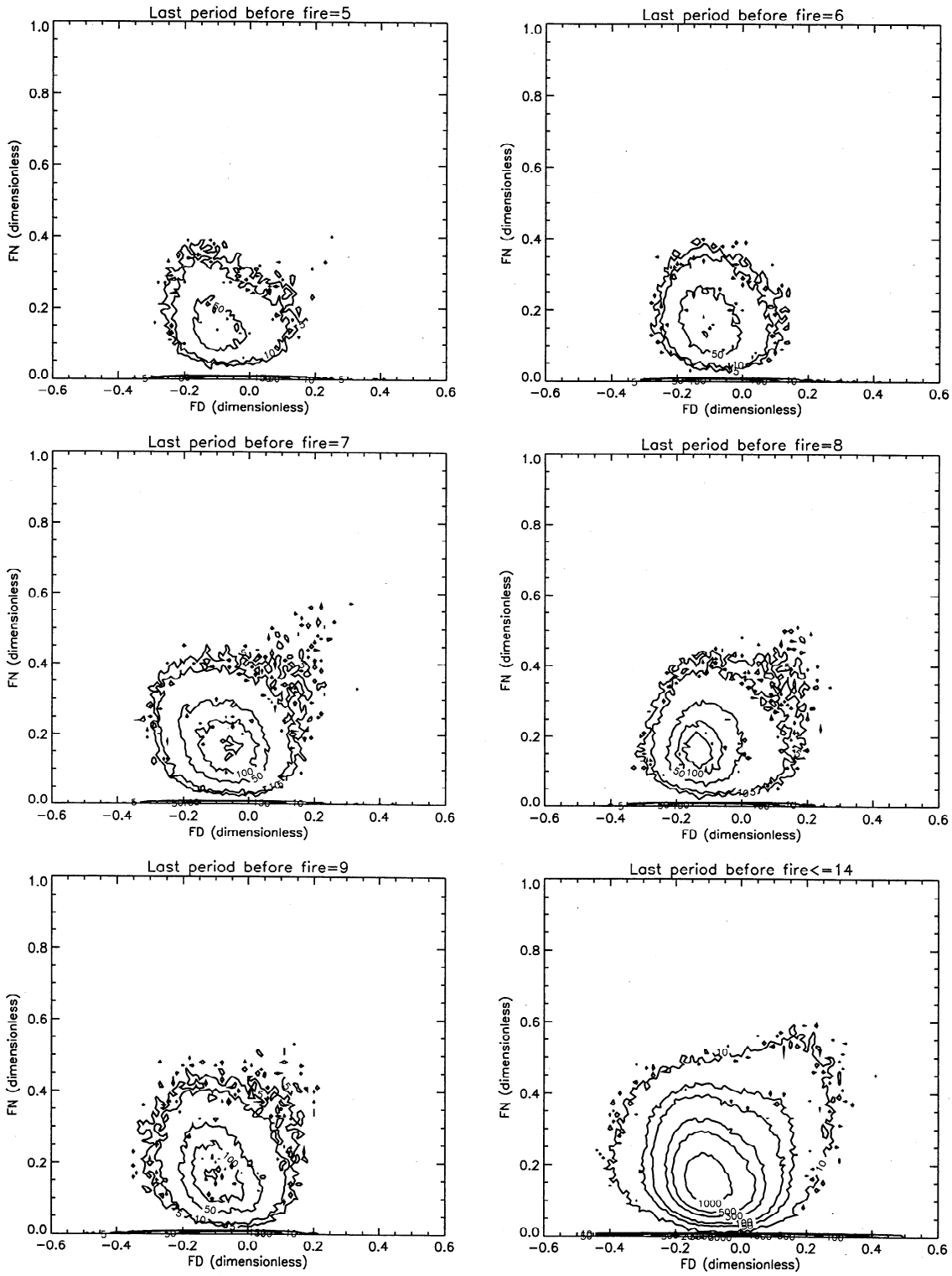

Figure 1. A contour plot of pixel-by-pixel values for the maximum NDVI decrease (FN) versus the difference (1993 minus 1994) in the area under the annual NDVI curve (FD).

reduce some of the noise delineated by the large scatter of data points.

Using such scatter diagrams as those in Figure 1, a series of thresholds were derived to estimate the probability that a particular pixel was burned. Three sets of four linear equations were employed to specify thresholds in the FN versus FD space, each equation with a different slope and/or offset (see Appendix). The slopes and offsets were established on the basis of the 1994 data of central Canada. Using a set of decision rules, the probabilities derived from each set of thresholds were combined into a final probability that a given pixel was damaged by a fire. The adequacy of the thresholds and the final combination were checked by a visual comparison with the input FN and FD (1993 minus 1994) images and a comparison

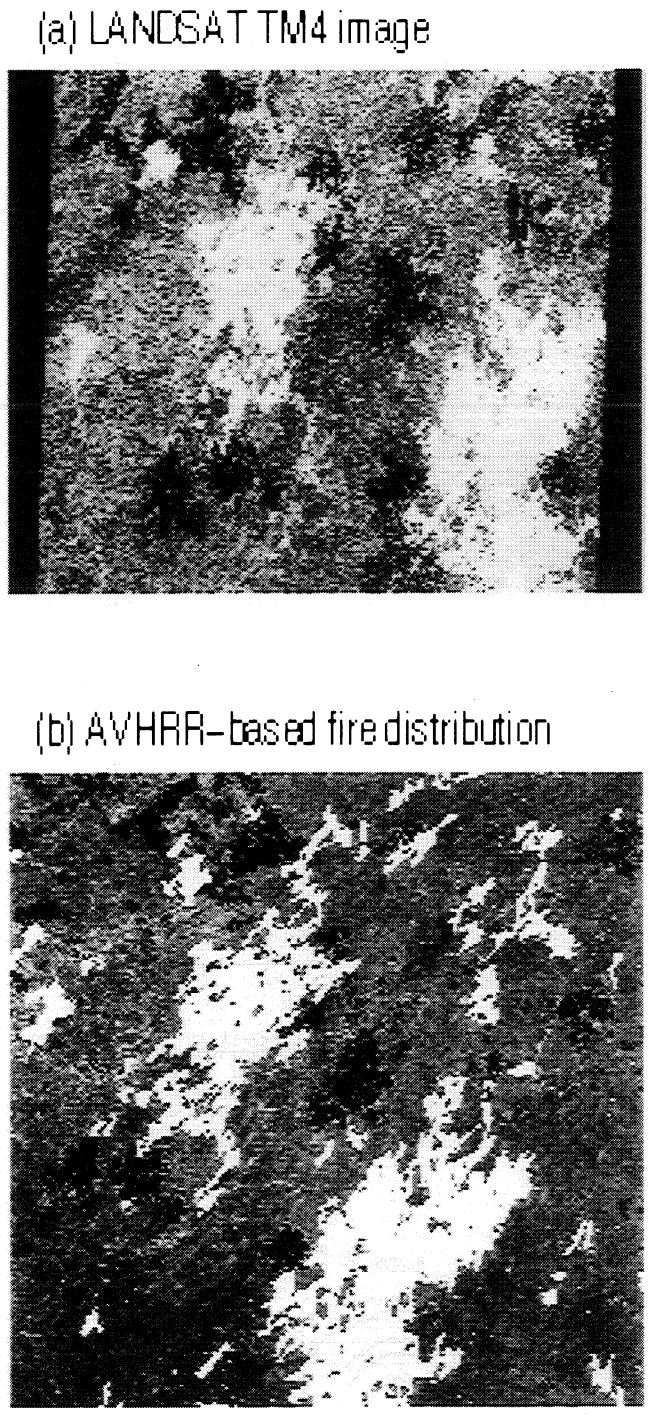

Figure 2. Comparison of the burned areas as indicated by the scars (dark regions) on (a) the Landsat TM4 image taken on May 14, 1995, with those detected using (b) AVHRR composite data in 1993 and 1994. The background in Figure 2b denotes the difference of the annual total NDVI between 1994 and 1993.

with some Landsat thematic mapper (TM) images obtained over the most heavily burned area.

Figure 2 provides an example of the comparison. The Landsat image (Figure 2a) shows the radiance in TM4 acquired over a region of 210 km × 210 km centered at N58°00′54″ and W103°00′59″ on May 16, 1995, when patchy snow cover over land and extensive snow cover over frozen lakes are clearly visible as white. The dark areas in Figure 2a outline the burned regions whose sizes, locations, and orientations correspond reasonably well with the dark areas in Figure 2b, which represent all AVHRR pixels identified as being fully or partly damaged by fires (i.e., final probability > 0). Note that the projections of Figures 2a and 2b are somewhat different (universal time meridian (UTM) and Lambert Conformal Conic), although this does not appreciably affect the different shapes. All well-delineated and contiguous fires of large burned areas seen in Figure 2a are also marked on Figure 2b. However, many scattered dark pixels in Figure 2b outside of the major burns are questionable. In contrast to the large number of small fires in the tropics [*Kaufman et al.*, 1990b], boreal forest fires tend to be low in number but generally extend over large areas [*Kasischke et al.*, 1993]. While some of the single pixels identified as fire may correspond to smaller burns, the majority of them are more likely to be false detection due to various sources of noise. The major source of noise in Figure 2b lies in the change of compositing procedure. In 1993, all pixels were eligible for compositing, while in 1994 only pixels within 57° from nadir were considered. Because of the maximum NDVI compositing criterion, mixed pixels at the edges of water bodies had apparently higher NDVI values in 1993, thus magnifying the 1993–1994 difference. This increase was sufficient to raise FD above the threshold values and alarming pixels near water bodies, especially in areas with high NDVI contrast. Note that many of the single pixels classified as fires are near water bodies (only large water bodies are shown in the image). Therefore only the larger, contiguous burned areas are discussed below.

2.2. Algorithm for Detecting Active Fires From Single-Day Images

Many algorithms have been developed to detect active fires using AVHRR measurements. Most of them were designed for applications in the tropics [*Kaufman et al.*, 1990b; *Arino and Mellnotte*, 1995], and few were applied to boreal forest [*Flannigan and Vonder Haar*, 1986]. In general, the algorithms that take advantage of the multichannel measurements from AVHRR in order to increase the confidence of detection and information content of a fire are similar in concept. For example, the method of *Kaufman et al.* [1990b] consists of three steps on the basis of channel 3 and 4 data. We tested the method and found that the essential information is contained in channel 3. The second and third tests of *Kaufman et al.* [1990b], designed to remove the effect of warm surface and clouds, did not play a significant role in the relatively colder environment of the BOREAS region but were used nevertheless since they did not seem to have any adverse effect.

AVHRR channel 3 is most sensitive to active fires because it tends to become saturated with the presence of small fires (fraction of a pixel). Depending on the sensor, calculated saturation brightness temperature in channel 3 ranges from 322 to 331 K [*Robinson*, 1991b]. Following an examination of burning areas (indicated by smoke in channel 1), we chose 316 K as the threshold, coincident with that used by *Kaufman et al.* [1990b]. As mentioned above, we also used the two other tests suggested by *Kaufman et al.* [1990b]: difference of brightness temperature between channel 3 and 4 larger than 10 K and brightness temperature in channel 4 larger than 245 K. The most prominent problem encountered in using these three tests is the false alarm due to Sun glitter. Sun glitter arises from specular reflection of the incoming solar radiation over many

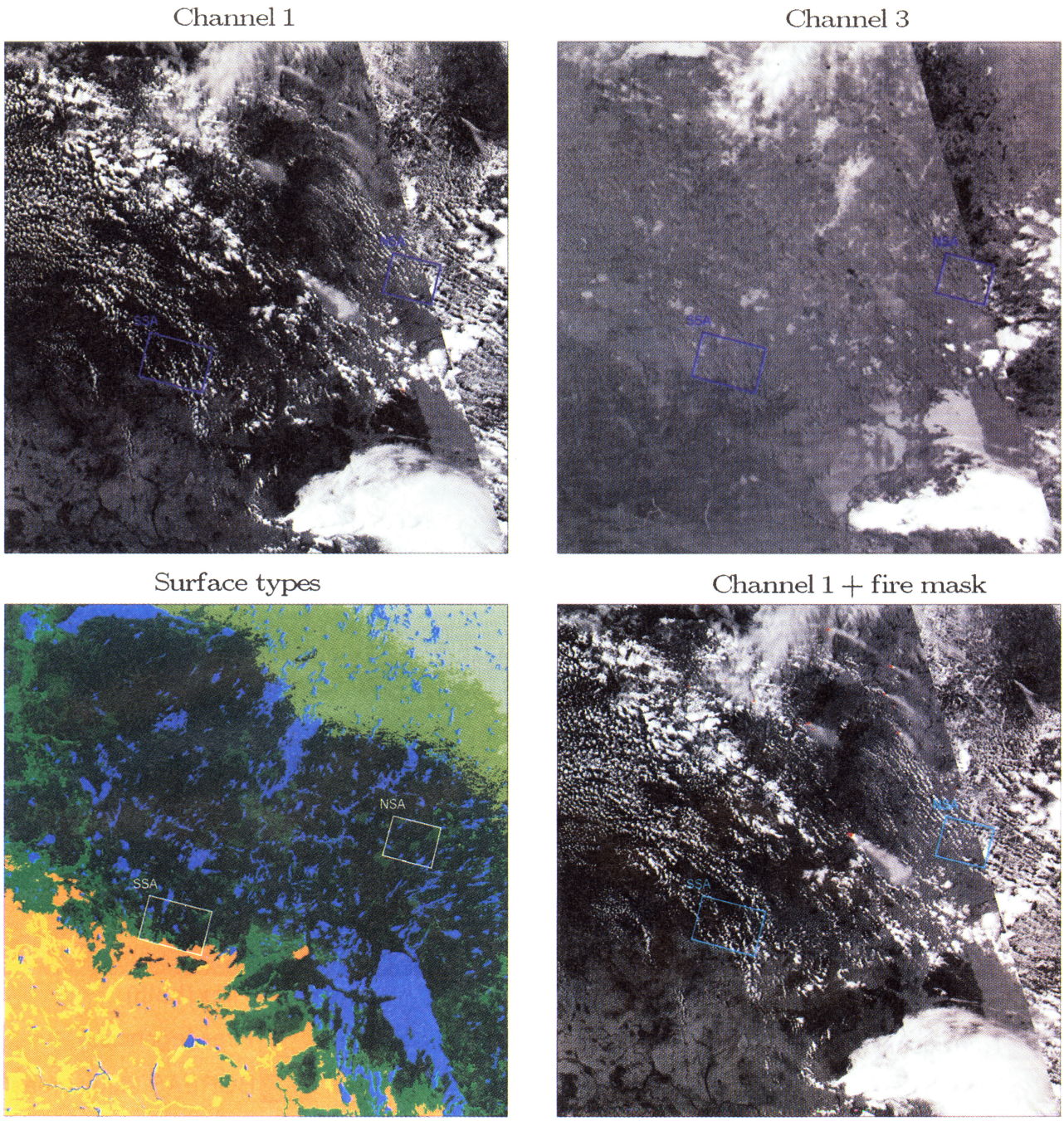

Plate 1. Single-day AVHRR images of (a) channel 1 reflectance, (b) channel 3 brightness temperature, (c) land cover type, and (d) fire masks (red) superimposed on channel 1 reflectance around the BOREAS study region on June 21, 1994.

objects, such as water bodies, snow, ice, swamp, bare soil, and clouds. There are several hundreds of lakes of various sizes and numerous rivers and swamps located across the BOREAS study region that are strong specular reflectors. In addition to saturation in channel 3, such pixels have high reflectance in channel 1 and 2 and low NDVI, which are all similar to the spectral characteristics of smoke. Therefore fire information in these channels is limited. For a flat object such as the calm water surface, sun glitter occurs at a view zenith angle similar to the solar zenith and a relative azimuth angle around 180°, that is, forward scattering. However, in reality, the phenomenon is often observed in many forward scattering directions near the principal plane, presumably because of the rough surface of a natural reflector. Therefore we simply discard all forward scattering measurements (the geometry is known for each pixel acquired). This may eliminate some fires, but this omission can be compensated to some extent by the overlapping of sun-synchronous orbits at latitudes as high as the BOREAS region and by visual inspection. We have tried other methods proposed to cope with this problem but have done so without much success. For example, *Arino and Mellnotte* [1995] added two more tests to the method of *Kaufman et al.* [1990b] to detect fires in Africa. They employed the reflectance in channels 1 and 2. If the reflectance in channel 1 is larger than

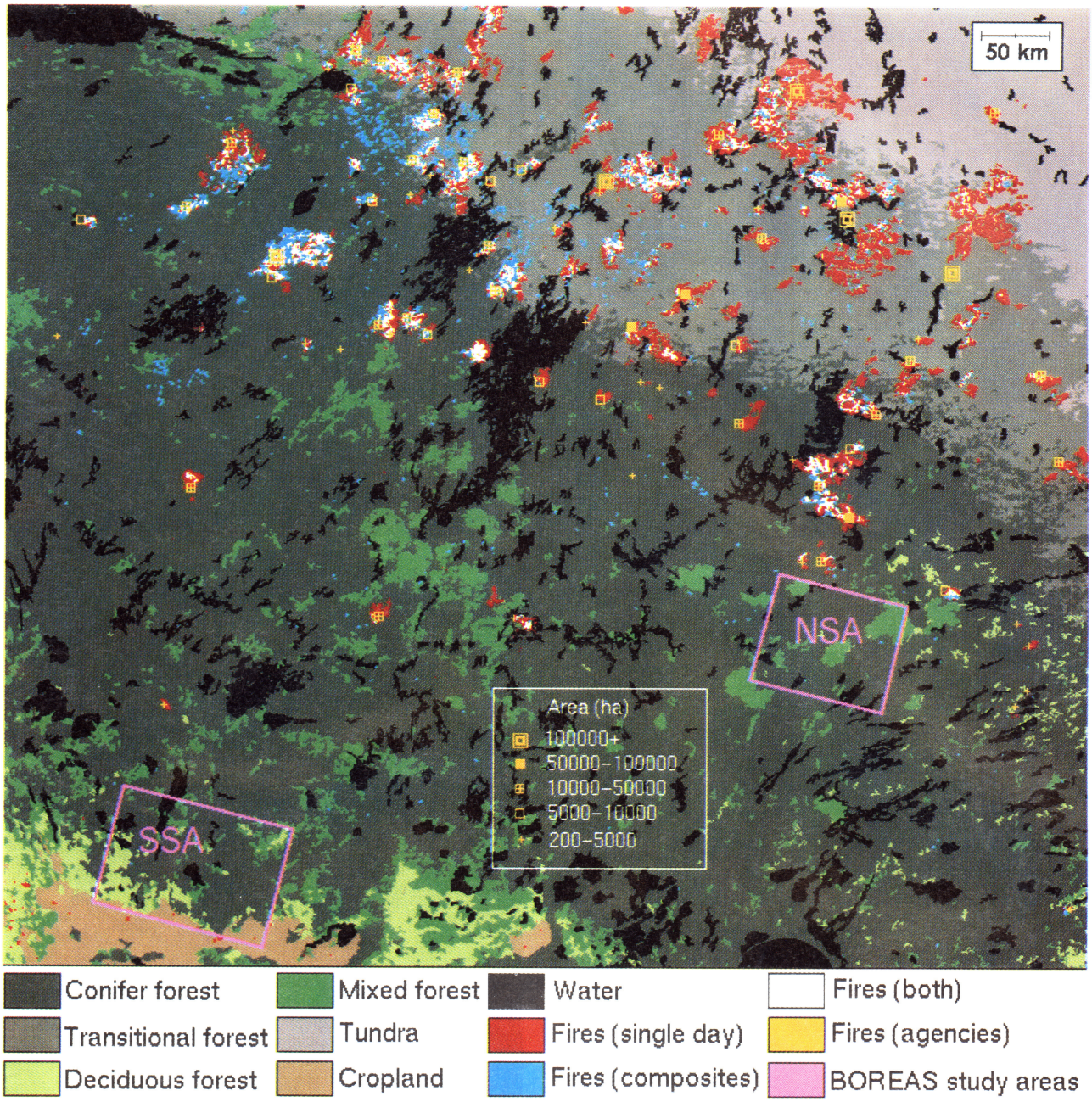

Plate 2. Fire distributions around the BOREAS region in 1994 observed at the surface (yellow) and detected by satellite using AVHRR composite data (blue) and single-day images (red). White color represent pixels identified as fires by the two satellite algorithms. Fire locations and areas reported at the surface are given by various yellow symbols.

0.25, they assume it is a bare soil pixel. If the absolute difference between the reflectance in channel 1 and 2 is less than 0.01, they assume it is a pixel contaminated by sun glitter over water. We tried their method but discovered that while it can eliminate some false alarms, it has the adverse effect of eliminating many real fires. Changing the threshold value does not seem to result in significant improvement. This is probably due to the fact that forest fires spawn a larger area and produce a lot of smoke compared to savanna fires. The smoke is bright in channels 1 and 2, and several fire pixels are eliminated by the tests designed to remove pixels contaminated by sun glitter. Masking water and bare soil pixels would, in principle, eliminate most of the pixels contaminated by sun glitter. Unfortunately, no mask information now available is precise enough. Besides, a lot of water bodies in northern Canada are of subresolution size, rendering masking ineffective.

The strengths and weaknesses of the single-day algorithm are demonstrated in Plate 1. Plates 1a and 1b show channel 1 reflectance and channel 3 brightness temperature, respectively, over the BOREAS region. The discontinuity separates the image into backward and forward viewing zones on the left and right portions of the images, respectively. They were taken from two consecutive satellite passes. Several fires are manifested in Plate 1a by the well-defined smoke plumes. However, unless a pattern recognition skill is invoked, it is hard to distinguish these plumes from clouds according to the radiometric

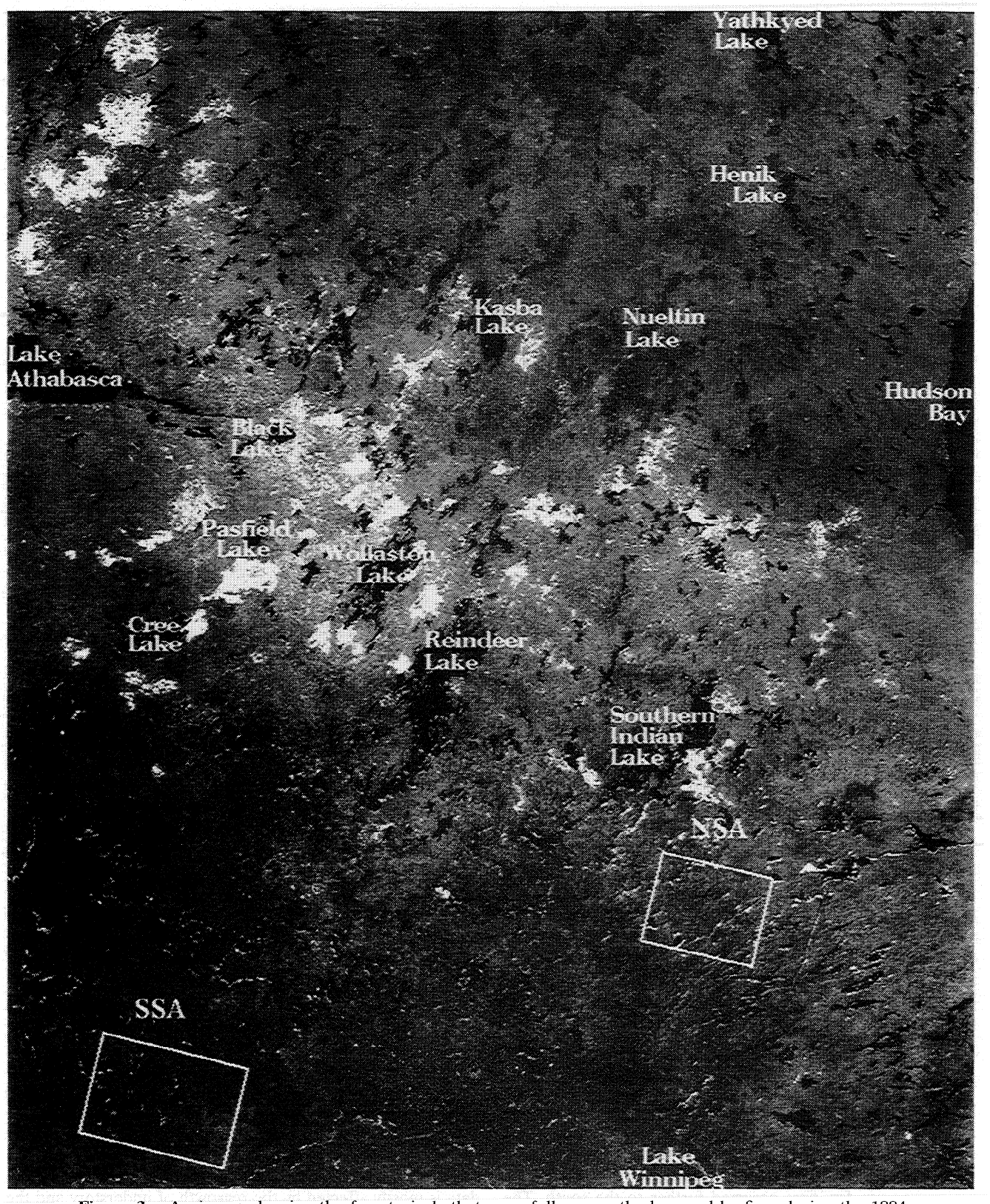

Figure 3. An image showing the forest pixels that were fully or partly damaged by fires during the 1994 growing season (white). The background is the difference in the area under the NDVI curve during the growing season between 1993 and 1994.

value. Moreover, fires do not always have such discernible smoke plumes/palls as exhibited here. In comparison, the locations of these fires are clearly marked on the channel 3 image (Plate 1b) as the darkest points representing high brightness temperature. Unfortunately, high brightness temperature is also observed at many other locations on the image of forward viewing geometry, corresponding mostly to lakes (Plate 1c). The lakes/rivers do not cause any confusion in the backward

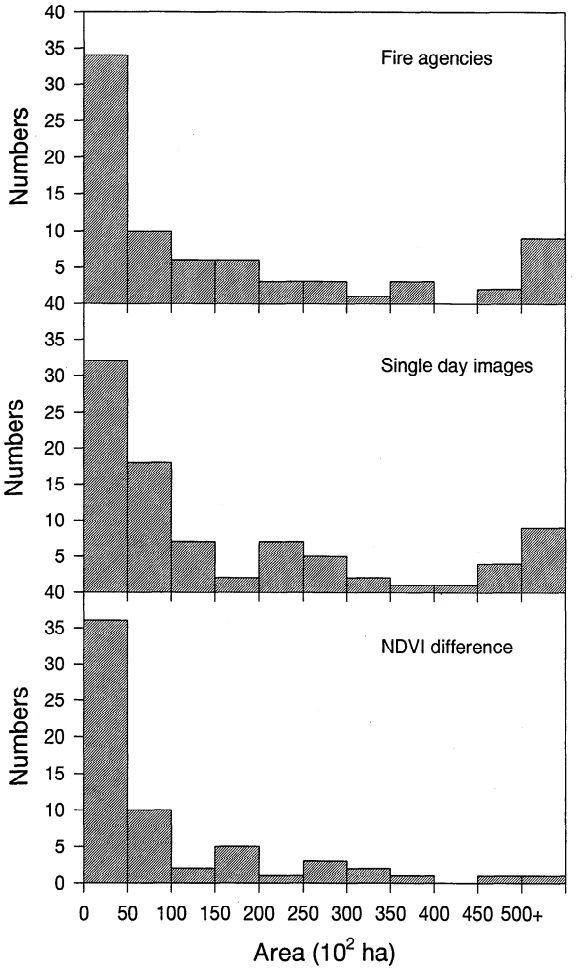

Figure 4. Histograms of the number of fires with varying burned areas reported at the surface (upper panel), estimated from single-day images (middle), and 10-day composites (lower).

viewing direction, as they have lower brightness temperatures than the surrounding land. Plate 1d is a combination of detected fires on top of the channel 1 reflectance image. The simple threshold method appears to detect most fires. It is worth noting that some fires under thin cloud cover are barely visible from the channel 1 image but have been identified by channel 3. A few fires in the forward scattering directions are missed.

3. Results and Discussion

A large volume of NOAA 11 AVHRR data were processed for this study. They include both 10-day composite data and single-day images in a region in central Canada. The region is slightly smaller than, and further north to, the BOREAS study region because few fires occurred further to the south. The southern agricultural area is excluded and the transitional forests north of BOREAS are included. Composite data were processed for the periods April to October, 1993, and April to September, 1994, when the AVHRR sensor onboard NOAA 11 failed. A detailed description of the processing methodology for AVHRR composites is given by *Cihlar et al.* [1997]. The processing removes or alleviates artifacts due to sensor degradation, atmospheric attenuation, cloud contamination, and bidirectional dependence. The end result consists of "cleaned" radiance in the five AVHRR channels, NDVI, three angles regarding illuminating and viewing geometry, and the date when the pixel was imaged. Single-day images were processed for summer (May 1 to September 10) 1994 only. Preprocessing single-day AVHRR data dealt with sensor calibration and registration only.

The algorithm described in section 2.1 was applied to the AVHRR composites in 1993 and 1994 for detecting total burned area in 1994. Fully or partly burned forest pixels in 1994 were identified and displayed in Figure 3 as white mask with the FD image as the background. The mask shows extensive burned areas along the transition zone between coniferous and transitional forests. In general, this region has higher values of FD than other parts of the image, implying that the growing condition in 1994 was worse than in 1993. Major burns were observed between Reindeer Lake and Black Lake and north of Lake Athabasca. Total burned area over the region is estimated to be 533,427 ha which excludes small burned areas (fewer than 5 pixels) that are questionable.

The algorithm for monitoring active fires was applied to single-day AVHRR images received in 1994. Hundreds of images were processed, and fire pixels on each image were identified. Plate 2 shows a comparison of the fire pixels identified using the single-day and composite AVHRR data. Except for some scattered small burned areas identified from the composite data, the agreement is fairly good in terms of the fire event. The fire location and area observed by fire agencies in the provinces of Manitoba and Saskatchewan are also displayed in Plate 3 as a quality check of the remote sensing techniques. Noting that the locations reported do not correspond to the center of a fire but where the fire was first spotted, the agreement is considered satisfactory.

Comparison of burned area is more difficult because of uncertainties in both satellite and ground data. For satellite detection the uncertainties stem from the problems inherent in remote sensing data and the algorithms. The single-day method tends to overestimate the area as a result of the saturation of channel 3, the degree of overestimation depending on the burned area and the flame temperature. On the other hand, the method could underestimate the burned area because it only sees the fires that are active when the satellite overpasses. The degree of underestimation is variable, depending on fire duration and movement. The low sampling rate of the sun-synchronous satellite could miss some short-lived fires. This problem could be resolved using the new generation geostationary satellite (GOES 8), which carries a midinfrared channel [*Prins and Menzel*, 1996], if it had a good spatial coverage and high resolution at high latitudes. Notwithstanding these problems, the final output of the burning area compares well with ground reports (see later discussion), partially because of the offset of the two opposing effects associated with the satellite method.

The performance of the algorithm on the basis of composite data is mostly affected by the regrowth of understory and the date of burning. If a fire occurs early in the season, the regrowth of vegetation may be sufficient to make up the loss in NDVI due to the burning, leading to the fire omission. Late in the season, phenological changes in greenness may be confused with senescence, especially farther in the north, where the growing season is short. Depending on the fire intensity and behavior, the degree of damage may be insufficient to cause a significant change in NDVI. A small ground fire may

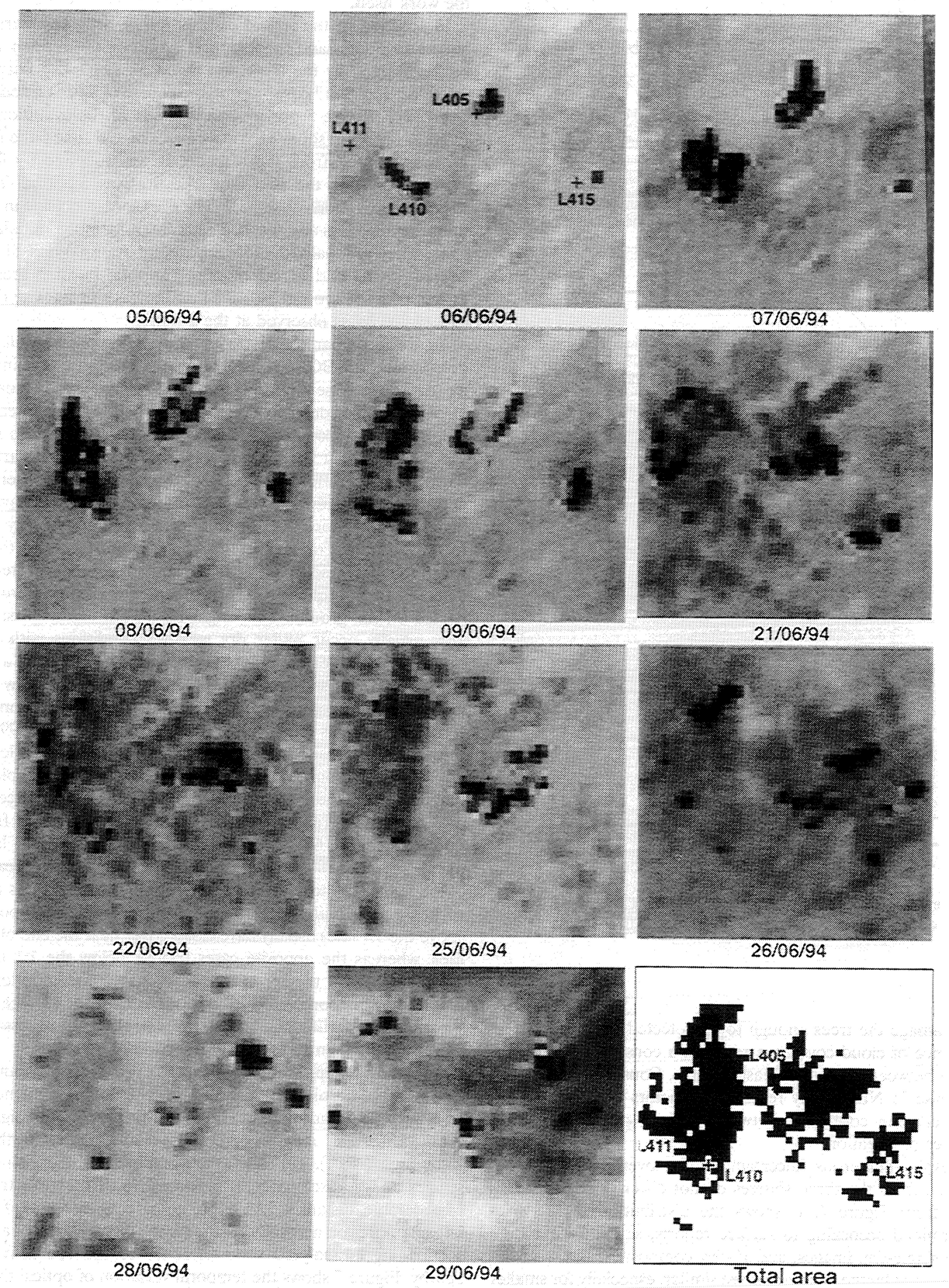

Figure 5. Temporal evolution of the fires near the south end of Wollaston Lake. The names of the fires assigned by fire agencies are marked on the image. The background of the image shows AVHRR channel 3 radiance, and the dark pixels are saturated or close to saturation. Each image is about 47 km × 47 km.

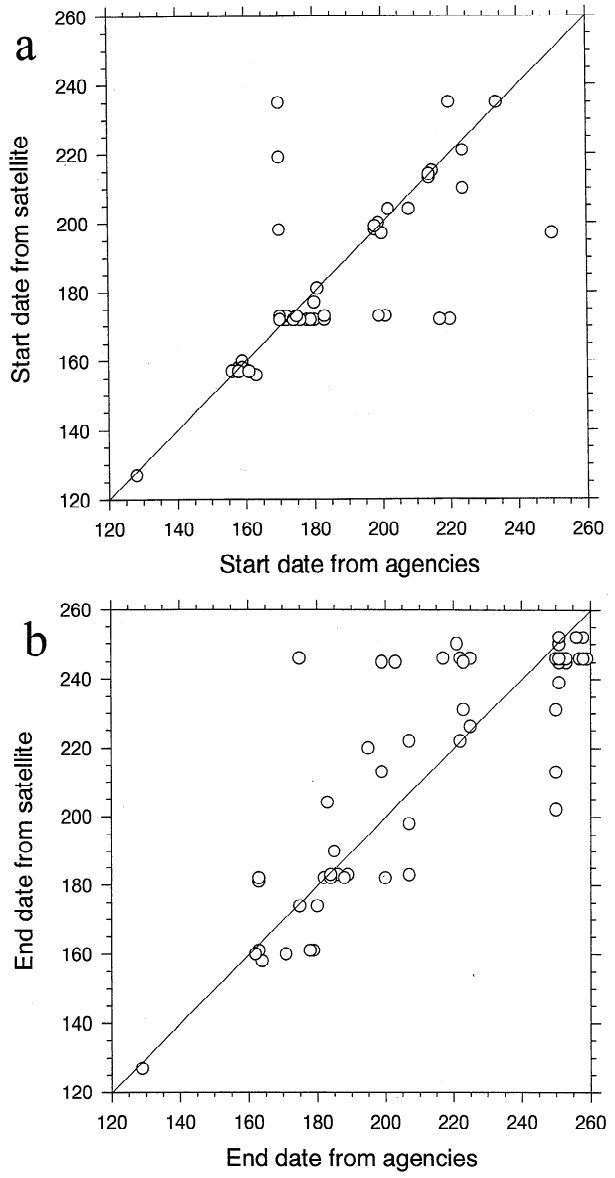

Figure 6. Comparison of fire (a) starting and (b) ending dates detected from space and observed at the surface.

not damage the trees enough to be detected from space. The presence of cloud cover can result in a considerable time interval between clear-sky measurements. Consequently, a large decrease in NDVI may result from factors other than fires, thus causing confusion between burned pixels and other sources of variation.

Despite numerous uncertainties, the overall fire statistics derived from the three sources do not differ drastically, as is seen from Figure 4. It shows the distribution of fire sizes determined according to surface reports, satellite estimation from single-day images, and 10-day composites. Fire size statistics given by the histograms are similar, especially for smaller burns. For example, the number of fires with burning area less than 5000 ha is 33, 34, and 36 from the three sources. Nearly half of the fires have a size smaller than 10,000 ha. The greatest discrepancy was due to the underestimation of large fires by the seasonal NDVI-based algorithm. This may be attributed to the factors mentioned above and to the preliminary nature of the work itself.

In addition to the spatial distribution of fires, the starting and ending dates and the temporal evolution of fires can also be determined by the algorithm based on single-day images, provided that cloud cover during the course of a fire episode is not severe. Figure 5 provides an example of the evolution of the fires observed south of Wallaston Lake. On June 5 the first fire was spotted from the satellite. It was followed by four separate fires on the next day. The fire was reported from surface observations on June 7. The fires spread quickly in the following few days and reached peak intensity in the middle of June. They gradually diminished around June 20 and disappeared by the end of the month. The total burning area is estimated to be around 56,000 ha on the basis of satellite data and 49,000 ha as observed at the ground.

Figure 6 compares the starting and ending dates of all the fires around the BOREAS study region detected using single-day data with those reported at the surface. While the accuracy of burning dates determined from the satellite is hindered by the presence of cloud cover, the comparison presented in Figure 6a shows that the majority of satellite-based fire starting dates generally differ by only a few days from surface observed dates. There are about eight cases in Figure 6a whose starting dates differ by more than 1 month. These are more likely due to the mismatch of fires observed at the surface and those monitored from space. It is important to note that satellite detected fires frequently occurred earlier than they were reported on the ground. This might be due to two factors: (1) fires usually occur under dry weather conditions with few clouds, and (2) the amount of burning at the beginning of a fire is so small or in such remote areas that it may not draw the attention of surface observers. Conversely, AVHRR channel 3 can detect a fire as small as 10×10 m^2 [*Kaufman et al.*, 1990a]. Thus satellite monitoring is indispensable to earlier fire detection, even if a ground-based fire monitoring system is in place. In comparison, there are no apparent systematic differences in the ending dates reported at the surface and determined from satellites (Figure 6b). Note that fires with ending dates later than September 10 are not included in the comparison because of the failure of the AVHRR scanner on NOAA 11. Fires with earlier ending dates determined from the satellite (points above the 1:1 line) usually have cloud cover near the end of the fires, whereas the opposite cases (points below the 1:1 line) might be due to the termination of surface fire monitoring before they are completely extinguished. Thus the surface observations of starting and ending fire dates are not necessarily more reliable than the satellite observations.

An important application of the active fire data is to examine the impact of burning on BOREAS measurements. Depending on wind speed and direction, many of the fires could significantly affect the measurements, especially in the northern study area (NSA). Unless washed out by rain, the chemical species and aerosol particles produced from fires can travel considerable distances. As a preliminary assessment of the impact of fires on aerosol measurements, the variation of aerosol loading is analyzed with reference to the fire activities nearby. Figure 7 shows the temporal variation of optical thickness observed by a team from the NASA Goddard Space Flight Center led by B. Markham (RSS-11) at NSA for the period from May 18 to November 1, 1994. The day-to-day variation in aerosol loading is too large to be caused by natural fluctuation (dust outbreaks or severe pollution are highly unlikely in this

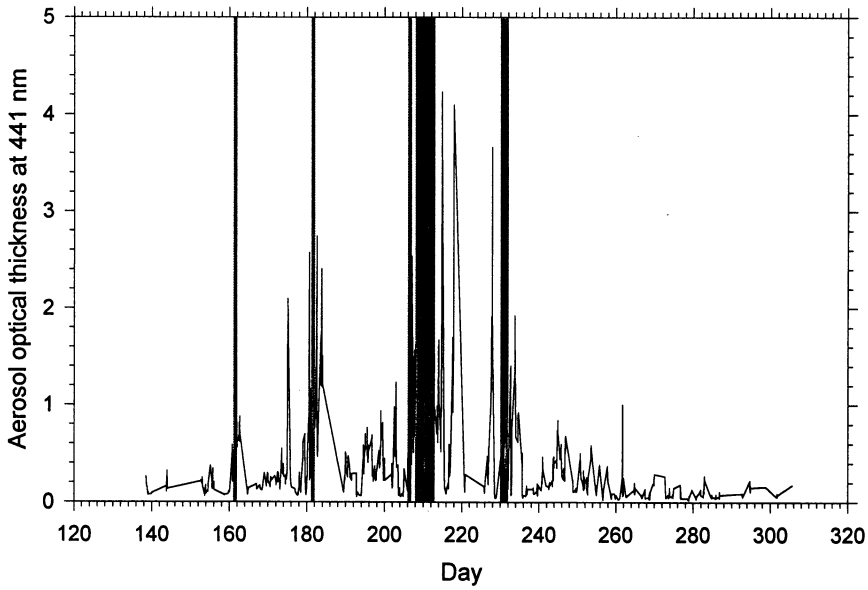

Figure 7. Day-to-day variation of aerosol loading at 441 nm observed at the northern study area (NSA). The grey bands indicate days for which heavy smoke was blown south from the fires depicted on Figure 8.

remote boreal forest region). The fire activities near NSA appear to support the argument that fire smoke is responsible for the fluctuation of the aerosol measurements.

Plate 3 shows the temporal evolution of fire locations detected by AVHRR channel 3 and the associated smokes visible from channel 1 reflectance. The fires took place between north of NSA and south of the Southern Indian Lake. The southern edge of the image corresponds to the northern bound of the NSA. The distance between the fires and the BOREAS observation sites ranges from less than 30 km to over 100 km. The fires could therefore seriously modify the measurement of aerosol optical thickness. If the wind is strong and blows toward the observation site, fires further away may also have an effect. Comparison between Figure 7 and Plate 3 reveals a good correspondence between the aerosol loading, fire occurrence, and smoke coverage. Note that some relatively low aerosol loads are not necessarily due to the absence or weakening of fire activities but may be explained by changing wind direction. Heavy smoke extends well into the NSA for many days, notably on June 10, June 30, July 24–30, and August 18–19. These periods correspond to unusually high aerosol loads. Similarly, one is expected to find fire impact on the measurements of other parameters such as radiative flux and trace gases.

4. Summary

Fire is an intrinsic part of the boreal forest ecosystem. It has a fundamental role in the growth and development of forest stands and their distribution across the landscape. This study is concerned with fire monitoring around the BOREAS study region during summer 1994 using AVHRR satellite data together with ground fire reports made by the provincial fire agencies of Saskatchewan and Manitoba. The fire information resulting from this study is particularly useful in analyzing BOREAS measurements of many parameters and understanding the processes and mechanisms that are responsible for the interaction between the atmosphere and the boreal forest.

Two different satellite algorithms were applied using AVHRR 10-day clear composites and single-day images. The composite algorithm identifies burned area on an annual basis, while the single-day technique detects burning pixels for each clear day. The former technique relies on changes in the NDVI from one composite period to another and from one year to the next, and the latter algorithm uses the channel 3 of AVHRR for pixels that are viewed from backscattering directions. The satellite data processed for this study include AVHRR composites from April to September in 1993 and 1994 and single-day data from May to September in 1994.

Attention was paid mainly to fires larger than 200 ha. Smaller fires are subject to large uncertainties and are difficult to compare among the three sources. A combination of ground-based and space-borne observations detected 99 fires. Surface observation reported 76 fires, 66 of which were detected from single-day AVHRR data and 60 of which from composite data. In addition, the single-day and composite techniques identified 13 and 14 more fires, respectively, that were not reported by the surface observers. The total burned area over the study region of about 56 million ha amounts to 1.82 and 1.97 million ha, respectively, according to surface reports and satellite-based detection using AVHRR single-day data. The bulk statistics of fire sizes are also close between the two methods, although individual fire size may differ a lot. The burned area detected on the basis of clear-sky composite data is substantially smaller than the above estimates because of numerous sources of uncertainty. In addition to burning area, the single-day method also provides information on the evolution of a fire. The fire starting dates detected by satellite are generally earlier than those reported at the surface. There is no apparent systematic difference in the fire ending date. Most of the fires were found along the transitional zone between conifer forests and transitional forests. Some fires are so close to the BOREAS sites that they might affect some measurements during the campaigns in the summer of 1994.

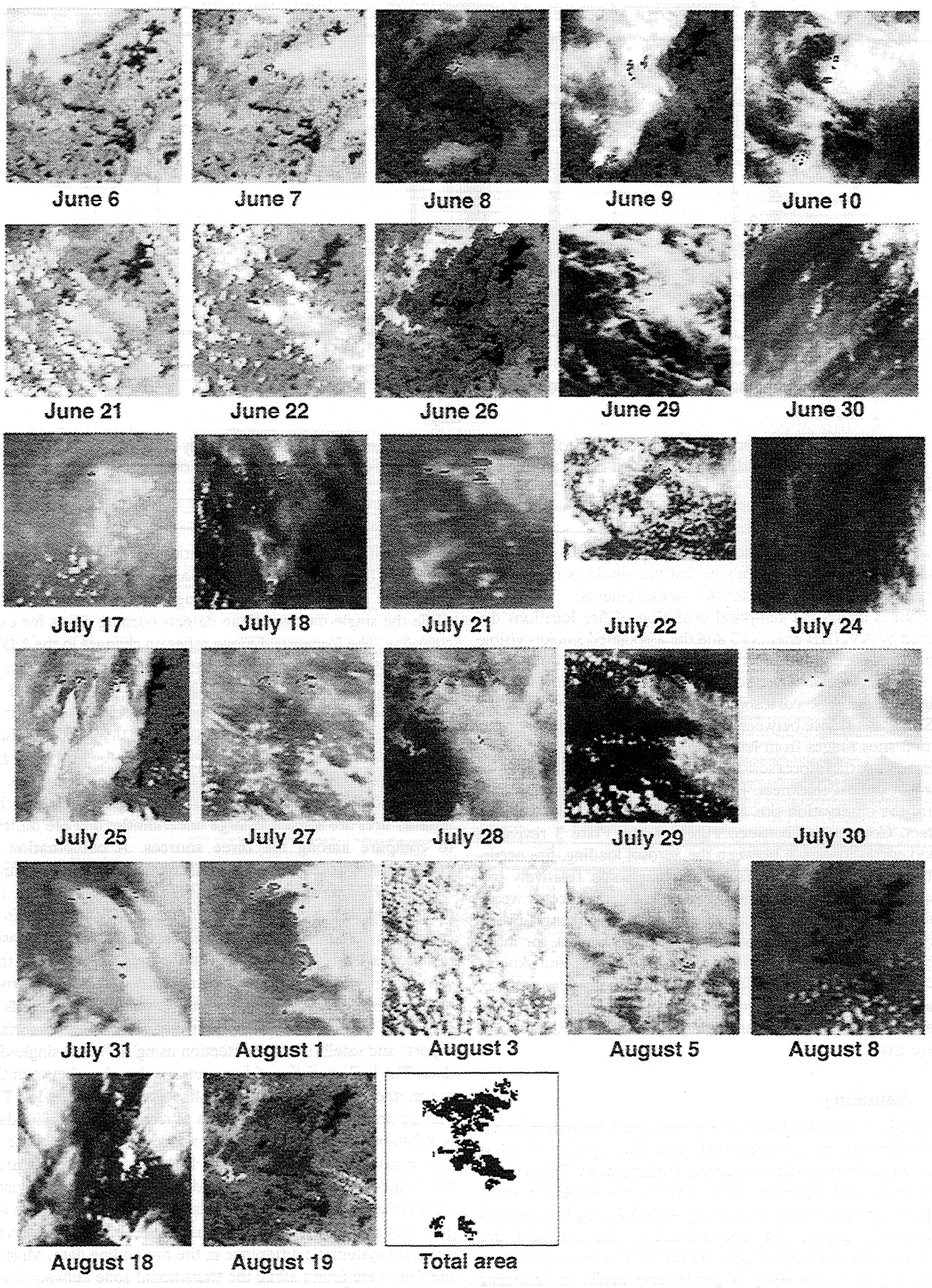

Plate 3. Evolution of fire locations detected by AVHRR channel 3 (red spots) with a background denoting channel 1 reflectance for the fires observed north of NSA. Each image is about 100 km × 100 km.

Appendix: Algorithm for Detecting Burned Pixels Using AVHRR Clear-Sky Composite Data

In principle, burned pixels should be readily detected from a decrease in NDVI after fire. However, in reality there are various complications: The decrease may not be strong enough, or not rapid enough, or may not be evident soon enough, to make the detection reliable. Thus the detection of burned areas in image composites must cope with occasionally weak signals and various sources of noise. The procedure designed here aims to cope with various sources of noise in the relationships (1) between fire and vegetation damage and (2) between vegetation damage and the ensuing remote sensing signal. It is based on two parameters, FN and FD, computed from the seasonal variation of NDVI.

FN Calculation

FN denotes the change of NDVI before and after a fire occurs, and $\Delta\text{NDVI}(i, j)$, normalized by the value of NDVI before the fire, that is,

$$\text{FN}(i, j) = \Delta\text{NDVI}(i, j)/\text{NDVI}_b(i, j) \quad \text{(A1)}$$

$$\Delta\text{NDVI}(i, j) = \text{NDVI}_b(i, j) - \text{NDVI}_a(i, j) \quad \text{(A2)}$$

where NDVI_b and NDVI_a are the mean NDVI values before and after the fire for a pixel (i, j) in the same growing season. Note that (A1) is valid only if $\Delta\text{NDVI}(i, j)$ is larger than the median value ($\text{M}(i, j)$) of the absolute differences between the measured and estimated NDVI; otherwise, FN is simply set to zero. The reason for using $\text{M}(i, j)$ as a threshold is to avoid false alarms caused by a "natural" noise in NDVI estimation. $\text{M}(i, j)$ was obtained using a Fourier approximation to the NDVI curve over the growing season [*Sellers et al.*, 1994; *Cihlar*, 1996].

After identifying the pixels contaminated by clouds or other atmospheric effects [*Cihlar*, 1996], the potential fire event in each pixel was found as the 10-day period with the highest NDVI decrease during the growing season. NDVI_b and NDVI_a were then computed from the values of NDVI for three clear-sky compositing periods (10 days each) preceding and following the fire event. This was done by discarding the lowest (for NDVI_b) or highest (for NDVI_a) value and averaging the remaining two values. The three periods were again used to reduce the "natural" noise in NDVI estimation. If there was insufficient number of clear sky measurements, NDVI_b (NDVI_a) was simply taken to be the highest (lowest) NDVI among the available values during the three periods before (after) the fire. The magnitude of the NDVI decrease relative to the "background" $\text{NDVI}(i, j)$ fluctuation quantified by $\text{M}(i, j)$ then determines whether a fire event was likely (see (A1) and the discussion below).

FD Calculation

FD measures the difference in the total area under the NDVI curve during the growing season between the year under study (1994 in this case) and the preceding year (1993) (ΔTNDVI), normalized by the NDVI area for the year of interest (TNDVI):

$$\text{FD}(i, j) = \Delta\text{TNDVI}(i, j)/\text{TNDVI}(i, j, 1994) \quad \text{(A3)}$$

$$\Delta\text{TNDVI}(i, j) = \text{TNDVI}(i, j, 1993) - \text{TNDVI}(i, j, 1994). \quad \text{(A4)}$$

Table A1. Coefficients for Threshold Lines to Quantify the Likelihood of Burned Pixels in Image Composites

Coefficient	$k, m, n = 1$	$k, m, n = 2$	$k, m, n = 3$	$k, m, n = 4$
a_1	−0.73	−0.73	−0.73	−0.73
a_2	−1.81	−1.81	−1.81	−1.81
b	0.7	0.6	0.5	0.4
b_1	0.7	0.6	0.5	0.4
b_2	1.0	0.81	0.64	0.45

FD thus describes the cumulative impact of a fire on the NDVI.

In principle, either FN or FD should suffice to identify the fire event in a pixel. In reality, however, the fire signal conveyed in the two parameters is distorted by various sources of noise. Since the two measures rely on different aspects of the NDVI temporal trajectories, they balance the noise sources in the data. If these two measures were highly correlated, the scattergram would approximate a line. As Figure 1 shows, this is not the case. Since the burned pixels have high FN and high FD values, they should be located in the upper right corner of the FN versus FD scattergrams. In practice, they follow the curvilinear contours evident in Figure 1. A threshold separating the burned pixels should thus be based on higher-order polynomial functions to follow the contours. Since the shapes of the scattergram vary from case to case, we employed a series of straight lines instead. The idea is to "slice off" increasingly larger portions of the scattergram (starting in the top right-hand portion), with each of these having a lower probability of being a burned pixel.

Computation of the Probability of the Pixel Being Burned

Three sets of lines were designed to quantify the probability of a pixel being burned on the basis of the FN value (PBN), FD value with a higher FN (PBD), and FD with a lower FN (PBS):

$$\text{PBN}(k) = b(k), \quad \text{(A5)}$$

$$\text{PBD}(m) = a_1 \times \text{FD}(i, j) + b_1(m) \quad \text{(A6)}$$

$$\text{PBS}(n) = a_2 \times \text{FD}(i, j) + b_2(n); \quad \text{(A7)}$$

where a and b denote slope and intercept of each line; and k, m, and n refer to the discriminant line. Their values are given in Table A1.

The PBN series identifies pixels with very high FN values. PBD identifies those with lower FN values and high FD. PBS is similar to PBD but with even lower values of FN and higher values of FD. Thus each function concerns a sub-portion of the scattergram, and the lines given by (A5)–(A7) slice progressively more into the scattergram, depending on the offset b_i. As b_i decreases, the likelihood of the pixel being burned also decreases. The specific values were chosen somewhat arbitrarily with the intent to capture the pixels in the upper right portion of the scattegram as shown in Figure 1.

On the basis of the above discriminant functions, the probability of a pixel being burned (as estimated by each of these partial criteria) was assumed to be equal to:

1.0 if

$$\text{PB}x > \text{PB}x(4) \quad \text{(A8)}$$

0.75 if

$$PBx(3) < PBx \leq PBx(4) \quad \text{(A9)}$$

0.5 if

$$PBx(2) < PBx \leq PBx(3) \quad \text{(A10)}$$

0.25 if

$$PBx \leq PBx(2), \quad \text{(A11)}$$

where PBx is PBN, PBD, or PBS.

For a final estimate of the likelihood of the pixel being burned, the three values resulting from (A8)–(A11) were added and divided by 2. The resulting probability classes for burned pixels were thus ≥1.0, 0.75, 0.5, 0.25, and 0. Pixels with these probabilities could then be displayed as an image.

Acknowledgments. The authors wish to thank Paul Maczek (Saskatchewan) and Peter Konepelny (Manitoba) for providing the wildfire occurrence data used in this study. Constructive comments were made by two reviewers (Y. J. Kaufman and C. Justice). J. Chen provided a CCRS internal review.

References

Arino, O., and J. M. Mellnotte, Fire index atlas, *Earth Obs. Quat.*, *50*, 11–16, 1995.

Brustet, J. M., J. B. Vickos, J. Fontan, K. Manissadjan, A. Podaire, and F. Lavenu, Remote sensing of biomass burning in West Africa with NOAA-AVHRR, in *Global Biomass Burning*, edited by J. S. Levine, pp. 47–52, MIT Press, Cambridge, Mass., 1991a.

Brustet, J. M., J. B. Vickos, J. Fontan, A. Podaire, and F. Lavenu, Characterization of active fires in West Africa savannas by analysis of satellite data: Landsat Thematic Mapper, in *Global Biomass Burning*, edited by J. S. Levine, pp. 53–60, MIT Press, Cambridge, Mass., 1991b.

Cahoon, D. R., Jr., B. J. Stocks, J. S. Levine, W. R. Cofer III, and K. P. O'Neill, Seasonal distribution of African savanna fires, *Nature*, *359*, 812–815, 1992.

Charlock, T. P., and T. D. Sellers, Aerosol effects on climate calculations with time dependent and steady state radiative convective models, *J. Atmos. Sci.*, *37*, 1327–1337, 1980.

Christopher, S. A., D. V. Kliche, J. Chou, and R. M. Welch, First estimates of the radiative forcing of aerosols generated from biomass burning using satellite data, *J. Geophys. Res.*, *101*, 21,265–21,273, 1996.

Chuvieco, E., and R. G. Congalton, Mapping and inventory of forest fires from digital processing of TM data, *Geocarto Int.*, *3*, 41–53, 1988.

Chylek, P., and J. Wong, Effect of absorbing aerosols on global radiation budget, *Geophys. Res. Lett.*, *22*, 929–931, 1995.

Cihlar, J., Identification of contaminated pixels in AVHRR composite images for studies of land biosphere, *Remote Sens. Environ.*, *56*, 149–163, 1996.

Cihlar, J., H. Ly, Z. Li, J. Chen, H. Pokrant, and F. Huang, Multitemporal, multichannel AVHRR data sets for land biosphere studies: Artifacts and corrections, *Rem. Sens. Environ.*, *60*, 35–57, 1997.

Crutzen, P. J., L. E. Heidt, J. P. Krasnec, W. H. Pollock, and W. Seiler, Biomass burning as a source of atmospheric gases, CO, H_2O, N_2O, NO, CH3CL and COS, *Nature*, *282*, 253–256, 1979.

Dozier, J., A method for satellite identification of surface temperature fields of subpixel resolution, *Remote Sens. Environ.*, *11*, 221–229, 1981.

Flannigan, M. D., and T. H. Vonder Haar, Forest fire monitoring using NOAA satellite AVHRR, *Can. J. For. Res.*, *16*, 975–982, 1986.

Henderson-Sellers, A., K. McGuffie, and C. Gross, Sensitivity of global climate model simulations to increased stomatal resistance and CO_2 increases, *J. Clim.*, *8*, 1738–1756, 1995.

Hobbs, P. V., and L. F. Radke, Cloud condensation nuclei from a simulated forest fire, *Science*, *163*, 279–280, 1969.

Hudson, J. G., J. Hallett, and C. F. Rogers, Field and laboratory measurements of cloud-forming properties of combustion aerosols, *J. Geophys. Res.*, *96*, 10,847–10,859, 1991.

Justice, C., J. P. Malingreau, and A. W. Setzer, Remote sensing of fires: Potential and limitations, in *Fire in the Environment*, edited by P. J. Crutzen and J. G. Goldammer, pp. 77–88, John Wiley, New York, 1993.

Kasischke, E. S., N. H. F. French, P. Harrell, N. Christensen Jr., S. L. Ustin, and D. Barry, Monitoring of wildfires in boreal forests using large area AVHRR NDVI composite image data, *Remote Sens. Environ.*, *45*, 61–71, 1993.

Kasischke, E. S., L. L. Bourgeau-Chavez, N. H. F. French, P. Harrell, N. Christensen Jr., Initial observations on the use of SAR imagery to monitor wildfires in boreal forests, *Int. J. Remote Sens.*, *15*, 3–16, 1994.

Kaufman, Y. J., and T. Nakajima, Effect of Amazon smoke on cloud microphysics and albedo, *J. Appl. Meteorol.*, *32*, 729–744, 1993.

Kaufman, Y. J., C. J. Tucker, and I. Fung, Remote sensing of biomass burning in the tropics, *J. Geophys. Res.*, *95*, 9927–9939, 1990a.

Kaufman, Y. J., A. Setzer, C. Justice, C. J. Ticker, and I. Fung, Remote sensing of biomass burning in the tropics, in *Fires in the Tropical Biota, Ecosystem Processes and Global Changes*, edited by J. G. Goldammer, pp. 371–399, Springer-Verlag, New York, 1990b.

Kaufman, Y. J., D. Tanre, and D. E. Ward, Remote sensing of biomass burning in the Amazon, *Remote Sens. Rev.*, *10*, 51–90, 1994.

Li, Z., Influence of absorbing aerosols on the solar surface radiation budget, *J. Clim.*, in press, 1997.

Martin, M. P., and E. Chuvieco, Mapping and evaluation of burned land from multitemporal analysis of AVHRR NDVI images, *EARSEL Adv. Remote Sens.*, *4*(3), 7–13, 1995.

Menzel, W. P., E. C. Cutrim, and E. M. Prins, Geostationary satellite estimation of biomass burning in Amazonia during BASE-A, in *Global Biomass Burning*, edited by J. S. Levine, pp. 41–46, MIT Press, Cambridge, Mass., 1991.

Penner, J. E., R. E. Dickinson, and C. A. O'Neill, Effects of aerosol from biomass burning on the global radiation budget, *Science*, *256*, 1432–1434, 1992.

Pollard, D., and S. M. Thompson, The effect of doubling stomatal resistence in a global climate model, *Global Planet. Change*, *10*, 1–4, 1995.

Prins, E. M., and W. P. Menzel, Trends in South American biomass burning detected with the GOES VISSR radiometer atmospheric sounder from 1983 to 1991, *J. Geophys. Res.*, *99*, 16,719–16,735, 1994.

Razafimpanilo, H., R. Frouin, S. F. Iacobellis, and R. C. J. Somerville, Methodology for estimating burned area from AVHRR reflectance data, *Remote Sens. Environ.*, *54*, 273–289, 1995.

Robinson, J. M., Problems in global fire evaluation: Is remote sensing the solution?, in *Global Biomass Burning*, edited by J. S. Levine, pp. 67–76, MIT Press, Cambridge, Mass., 1991a.

Robinson, J. M., Fire from space: Global fire evaluation using infrared remote sensing, *Int. J. Remote Sens.*, *12*, 3–24, 1991b.

Sellers, P. J., S. O. Los, C. J. Tucker, C. O. Justice, D. A. Dazlich, J. A. Collatz, and D. A. Randall, A global 1° by 1° NDVI data set for climate studies, 2, The generation of global fields of terrestrial biophysical parameters from the NDVI, *Int. J. Remote Sens.*, *15*, 3519–3545, 1994.

Sellers, P., F. Hall, H. Margolis, B. Kelly, D. Baldocchi, G. den Hartog, J. Cihlar, M. G. Ryan, B. Goodison, P. Crill, K. J. Ranson, D. Lettenmaier, and D. E. Wickland, The boreal ecosystem-atmosphere study (BOREAS): An overview and early results from the 1994 field year, *Bull. Am. Meteorol. Soc.*, *76*, 1549–1577, 1995.

Stocks, B. J., The extent and impact of forest fires in Northern circumpolar countries, in *Global Biomass Burning*, edited by J. S. Levine, pp. 197–202, MIT Press, Cambridge, Mass., 1991.

Takana, S., H. Kimura, and Y. Suga, Preparation of a 1:25000 Landsat map for assessment of burnt area on Etajima Island, *Int. J. Remote Sens.*, *4*, 17–31, 1983.

Warner, J., and S. Twomey, The production of cloud nuclei by cane fires and the effects on cloud droplet concentration, *J. Atmos. Sci.*, *24*, 704–706, 1967.

J. Cihlar and Z. Li, Canada Centre for Remote Sensing, 588 Booth Street, Ottawa, Ontario, Canada K1A 0Y7. (e-mail: li@ccrs.emr.ca)

F. Huang and L. Moreau, Intermap Information Technologies, 588 Booth Street, Ottawa, Ontario, Canada K1A 0Y7.

B. Lee, Canadian Forest Service, 5320 122 Street, Edmonton, Alberta, T6H 3S5 Canada.

(Received May 28, 1996; revised March 3, 1997; accepted March 6, 1997.)